Functionalized Polypyrrole Film: Synthesis, Characterization, and Potential Applications in Chemical and Biological Sensors

Hua Dong,*,†,‡ Xiaodong Cao,†,‡ and Chang Ming Li*,§

Joint Department of Biomedical Engineering, North Carolina State University and University of North Carolina at Chapel Hill, Raleigh, North Carolina 27695, Center of Biomedical Engineering, School of Materials Science and Engineering, South China University of Technology, Guangzhou 510640, People's Republic of China, and Division of Bioengineering, School of Chemical and Biomedical Engineering, Nanyang Technological University, Singapore 637457, Singapore

ABSTRACT In this paper, we report the synthesis of a carboxyl-functionalized polypyrrole derivative, a poly(pyrrole-*N*-propanoic acid) (PPPA) film, by electrochemical polymerization, and the investigation of its basic properties via traditional characterization techniques such as confocal-Raman, FTIR, SEM, AFM, UV−vis, fluorescence microscopy, and contact-angle measurements. The experimental data show that the as-prepared PPPA film exhibits a hydrophilic nanoporous structure, abundant −COOH functional groups in the polymer backbone, and high fluorescent emission under laser excitation. On the basis of these unique properties, further experiments were conducted to demonstrate three potential applications of the PPPA film in chemical and biological sensors: a permeable and permselective membrane, a membrane with specific recognition sites for biomolecule immobilization, and a fluorescent conjugated polymer for amplification of fluorescence quenching. Specifically, the permeability and permselectivity of ion species through the PPPA film are detected by means of rotating-disk-electrode voltammetry; the specific recognition sites on the film surface are confirmed with protein immobilization, and the amplification of fluorescence quenching is measured by the addition of a quenching agent with fluorescence microscopy. The results are in good agreement with our expectations.

KEYWORDS: functionalized polypyrrole film • chemical and biological sensors • permeability and permselectivity • matrix for biomolecule immobilization • fluorescence quenching • electrochemical polymerization

1. INTRODUCTION

In the late 20th century, chemical and biological sensors have attracted considerable interest in both theoretical and practical aspects. A significant reason for the boomed development of these two sensors is the remarkable progress achieved in the field of polymeric materials and their relevant film preparation technologies. Nowadays, almost half of the promising chemical and biological sensors are based on polymers, and thousands of papers are being published each year involving the utilization of new polymers. Compared with other materials, polymers exhibit prominent advantages, including low cost, simple fabrication techniques, flexible deposition on various kinds of substrates, a wide choice of molecular structures, and the possibility to incorporate other materials into the bulk polymers or on its surface region for a vast variety of functional polymers with different physical and chemical properties (1). The role and/or effect of polymers in sensors can be summarized as dielectrics, a conductive composite, a probe immobilization matrix, electrolytes, sorbents, electroconducting conjugated polymers, ion-exchange membranes, permselective membranes, membranes with specific recognition sites, optically sensitive polymers, etc. (2).

As a typical conducting polymer, polypyrrole (PPy) is frequently used in electrocatalytic and affinity sensors and biosensors based on its unique electrical, optical, and thermal properties (3, 4). PPy can be synthesized via electrochemical polymerization, making it easier to determine the polymer structure and components in a controllable manner for diverse purposes. In order to further enlarge the application of PPy in sensors, much effort has been carried out in recent years to fabricate functionalized PPy derivatives through either modification of the pyrrole monomer's structure or the preparation of block and graft copolymers (5−10). The former method, namely, the synthesis of pyrrole monomer substituents, is very appealing because of the ease of polymerization and the wide variety of functional groups that can be linked to pyrrole, which enables post-functionalization of the resulting polymer. Another advantage of functionalized PPy derivatives is the enhanced fluorescent properties in comparison with PPy, indicative of their possible application in optical sensors.

This paper presents our recent work on the fabrication of a carboxyl-functionalized PPy derivative film, poly(pyrrole-*N*-propanoic acid) (PPPA), by electrochemical polymer-

* Corresponding authors. Tel.: 1-919-2710922 (H.D.), +65-67904485 (C.M.L.). Fax: 1-919-5156302 (H.D.), +65-67911761 (C.M.L.). E-mail: hdong2@ncsu.edu (H.D.), ecmli@ntu.edu.sg (C.M.L.).

Received for review April 20, 2009 and accepted June 23, 2009

† Joint Department of Biomedical Engineering, North Carolina State University and University of North Carolina at Chapel Hill.

‡ South China University of Technology.

§ Nanyang Technological University.

DOI: 10.1021/am900267e

ization. Its structure and morphology are investigated using confocal-Raman, Fourier transform infrared (FTIR), scanning electron microscopy (SEM), atomic force microscopy (AFM), UV−vis, fluorescence microscopy, and contact-angle measurements. Except for the regular characterization, in this work we emphasize, in particular, three potential applications of the PPPA film in a chemical and biological sensor permselective and osmotic membranes, membranes with specific recognition sites, and optically sensitive polymers (namely, fluorescent conjugated polymers). Their application-related properties are studied using specialized methods. Specifically, the permeability and permselectivity of ion species through the PPPA film are detected by means of rotating-disk-electrode (RDE) voltammetry, the specific recognition sites on the film surface are confirmed via protein immobilization, and the fluorescent sensitivity to the quenching agent is measured with fluorescence microscopy. To the authors' knowledge, this is the first time that fluorescence quenching of conducting polymers has been reported.

2. EXPERIMENTAL SECTION

2.1. Reagents and Materials. Pyrrole, a benzyltrimethylammonium hydroxide solution (40%), acrylonitrile, potassium hydroxide, hydrochloride acid, ethyl acetate, magnesium sulfate, methylene chloride, hexane, *N*-hydroxysulfosuccinimide sodium salt (NHS), phosphate-buffered saline (PBS), and 1,1′-dimethyl-4,4′-bipyridinium dichloride hydrate (paraquat dichloride) were purchased from Sigma-Aldrich, Inc. (Madison, WI). Chrompure mouse IgG and biotin-SP-conjugated affinipure sheep anti-mouse IgG $F(ab')_2$ were obtained from Jackson ImmunoResearch Laboratories (West Grove, PA). 1-Ethyl-3-[3-(dimethylamino)propyl]carbodiimide hydrochloride (EDC) was purchased from Pierce (Rockford, IL).

2.2. Synthesis and Characterization of PPPA Monomer. The synthesis of PPPA monomer, pyrrole-*N*-propanoic acid, is described in our previous work (11). Briefly, 3.8 mL of distilled pyrrole and 0.3 mL of benzyltrimethylammonium hydroxide were fully mixed, and then 2.9 mL of acrylonitrile was added slowly to avoid a temperature above 40 °C. After overnight stirring, the resulting mixture was hydrolyzed by the addition of 50 mL of potassium hydroxide (10 mol/L) and refluxed for 12 h. The solution was cooled down, and HCl was gradually added to acidify the solution to pH 3. The aqueous layer was extracted with ethyl acetate four times, each time with 30 mL of solvent. The combined organic layer was washed with 75 mL of brine and then dried with anhydrous magnesium sulfate. After solvent evaporation, the crude product was crystallized by methylene chloride and hexane. About 5 g of pure PPA monomer was obtained (65% yield). Other synthetic routes based on different reactants to prepare the PPPA monomer were also reported in the literature (12, 13).

The as-prepared product was identified by ^{1}H NMR and FTIR. ^{1}H NMR ($CDCl_3$, δ): 2.83 (t, $J = 7.2$ Hz, 2H), 4.20 (t, $J = 7.2$ Hz, 2H), 6.14 (t, $J = 2.1$ Hz, 2H), 6.67 (t, $J = 7.2$ Hz, 2H), 9.00 (s, broad peak, 1H). FTIR (KBr, cm^{-1}): 2938 (C−H, pyrrole), 1728 (−COOH, propanoic acid), 1504, 1433, and 1281 (pyrrole ring-stretching vibration), 1209, 1087, 935, and 727 (C−H, C−N in-plane and out-of-plane deformation vibrations).

2.3. Instrumentation. The electropolymerization and other electrochemical measurements were performed with an Autolab potentiostat/galvanostat apparatus (Eco Chemie BV, Utrecht, The Netherlands). The permeability of the PPPA film was investigated by rotating-disk-electrode (RDE) voltammetry (Pine Instrument, Grove City, PA). Field-emission scanning electron microscopy (SEM) was employed to examine the morphology

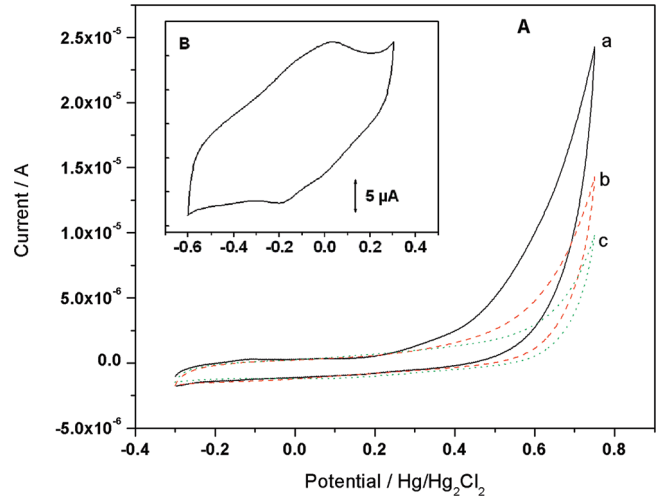

FIGURE 1. Electropolymerization via CV on a gold surface in 0.15 mol/L PPA monomer solutions with the potential range of −0.3 to +0.75 V vs SCE and a scanning rate of 50 mV/s: (a) first cycle; (b) fifth cycle; (c) 20th cycle. (Inset) CV curve of the electropolymerized PPPA film in 0.1 mol/L PBS.

change of gold electrodes before and after modification of the PPPA film. The photos were taken on a JEOL JSM-6700F (Tokyo, Japan) at an accelerating voltage of 5 kV and a working distance of 8 mm. Attenuated total reflection Fourier transform infrared (FTIR) spectra of an electropolymerized PPPA film were recorded with a Nicolet 5700 FTIR spectrometer (Thermo Electron Corp., Waltham, MA). Atomic force microscopy (AFM) was carried out to characterize the structure of the PPPA film and protein immobilization (Veeco Metrology Group, Santa Barbara, CA). Confocal-Raman microscopy (CRM200, WITec, Ulm, Germany) was used to observe the local fluorescent properties of the PPPA film with a spatial resolution of 0.2 μm. Fluorescence quenching of the polymer film in the presence of a quenching agent was detected on a fluorescence microscope (Olympus IX71). Detailed settings of RDE voltammetry and confocal-Raman microscopy are listed in the Supporting Information.

3. RESULTS AND DISCUSSION

3.1. Synthesis and Characterization of the PPPA Film. In our experiment, electropolymerization of the PPPA film was conducted by cyclic voltammetry (CV) on a gold electrode in a 0.3 mol/L PPA monomer solution. Figure 1 shows the first 20 scans in the potential range of −0.3 to +0.75 V vs saturated calomel electrode (SCE). Similar to the formation of the PPy film, there was an obvious current increase at the first oxidative scan (curve a) after the potential reached ∼0.2 V, which indicates electrooxidation of the pyrrole ring in the PPA monomer, in other words, deposition of the PPPA film on the gold surface. However, compared with PPy polymerization, where the anodic current in successive scans always remained the same or even larger than that in the first scan, the anodic current of PPPA polymerization decreased gradually with an increase of the CV cycles (curves b and c). To figure out this issue, the electrochemical behavior of the generated PPPA film in PBS was investigated and the data are given in Figure 1B (inset) (for comparison, the electrochemical behavior of the PPy film is shown in Figure S1 in the Supporting Information). Although the doping and undoping processes of PPPA could still be seen via a pair of redox peaks at 0.0

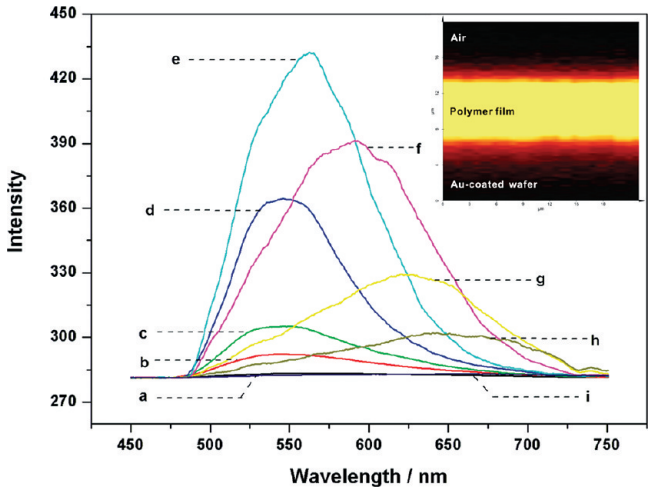

FIGURE 2. Confocal fluorescence spectra of the PPPA film with a thickness of 8 μm. Focal points: (a) 0 μm from the top of the polymer film, (b) 1 μm, (c) 2 μm, (d) 3 μm, (e) 4 μm, (f) 5 μm, (g) 6 μm, (h) 7 μm, and (i) 8 μm. (Inset) Fluorescence mapping in the depth profile of the PPPA film. The measurements were performed using a 100× oil immersion objective. The excitation wavelength was 488 nm.

and −0.2 V, the peak current was much lower relative to that of PPy, implying a poor conductivity of the PPPA film in contrast to that of PPy. As a result, further deposition of the PPPA film on a gold surface became more difficult with the growth of CV scans (corresponding to a decrease of the anodic current), and the whole polymerization turned out to be a self-control process.

On the basis of the above statement, it is conceivable that the low electrical conductivity of the PPPA film may affect the polymer chain length during the electropolymerization process; i.e., the chain length of the PPPA polymer (or molecular weight) varies with the growth of the film. The closer the PPPA molecule is to the electrode surface, the higher the chain length. Our opinion was proven by measuring the fluorescence emission (photoluminescence) of the PPPA film. As is well-known, the fluorescence spectrum of a conjugated polymer including the emission wavelength and intensity is strongly dependent on the polymer chain length (14−18). With the assistance of confocal technology, we are able to detect fluorescence spectra in different depths of the PPPA film and, therefore, identify the dependence of the polymer chain length on the film thickness (19, 20). Figure 2 shows the results of confocal fluorescence measurement. Except for the outermost and innnermost emission curves, where the laser light might be focused in the air and silicon substrate, all of the other curves exhibited a broad fluorescence emission peak. Comparably, the PPy film synthesized under the same experimental conditions showed almost no fluorescence emission. The main reason for the difference between the PPPA and PPy films is that the introduction of side chains to the PPy structure produces new local conformations, alters the $\pi-\pi$ electron delocalization, and thus leads to fluorescence emission in the visible region (16, 17, 21). Another interesting phenomenon observed in Figure 2 is the dramatic change of the fluorescence emission wavelength and intensity along the depth of the PPPA film. Red-shifted emission occurred when the focal point of the laser went from the outside of the PPPA film down to the electrode surface. In principle, "red" spectra are much more common for the polymers with longer chain lengths because longer chains can induce more easily the chain−chain contacts, as well as random chemical defects, and thus increase the numbers of low-energy exciton trap sites, resulting in red-shifted emission (22, 23). Hence, it is reasonable to speculate that the polymer chain length of the PPPA film is the highest in the electrode/polymer interface and gradually decreases with growth of the polymer film because of the poor electrical conductivity of the PPPA film. Once the chain length cannot be shortened any more for the solid PPPA film, i.e., the PPA monomer cannot be efficiently polymerized, the polymerization reaction is quenched automatically. In addition to red-shifted emission, the chain length of the conjugated polymer also plays a significant role in the efficiency of fluorescence emission (Table 1). Here the emission intensity maximum appeared at a wavelength of 564.2 nm (yellow) when the focal point was set at 4 μm deep from the top of the PPPA film. Higher or lower focal depths, namely, shorter or longer chain lengths, would weaken the fluorescence emission. Similar results were also reported on poly(*p*-phenylene) films by Vitukhnovsky et al. (18).

The fluorescence emission property of the PPPA film was further confirmed via fluorescence microscopy measurement. Because the absorption maximum of the PPPA film in UV−vis spectra occurred at 530 nm (see Figure S2 in the Supporting Information), a mercury vapor lamp with a FITC filter (~480 nm) was used as the excitation light source. Figure 3 shows the fluorescence image of the PPPA film synthesized on a transparent indium−tin oxide (ITO) electrode. No fluorescence emission was observed on bare ITO glass, as illustrated in Figure 3a. Meanwhile, the morphology of the electropolymerized PPPA film could be seen clearly in Figure 3b,c, indicating the strong fluorescence properties of this polymer.

The presence of carboxyl groups in the PPPA film was confirmed by FTIR spectroscopy, with the profile shown in Figure S3 in the Supporting Information. The absorbance peaks at 2938, 1504, 1433, and 1281 cm^{-1} in curve a (PPA monomer) could be ascribed to the C−H and C−C stretching vibration in the pyrrole ring, and the peaks at 1209, 1087, 935, and 727 cm^{-1} could be assigned to C−H and C−N in-

Table 1. Dependence of Fluorescence Emission on the Depth of the PPPA Film

	depth of the focal point from the top of PPPA film/μm								
fluorescence emission	0	1	2	3	4	5	6	7	8
emission maximum/ nm	540.6	544.7	546.2	548.4	564.2	592.2	623.2	643.4	661.0
relative intensity	1	5.5	12.0	41.5	75.5	54.5	24.0	10.5	1.5

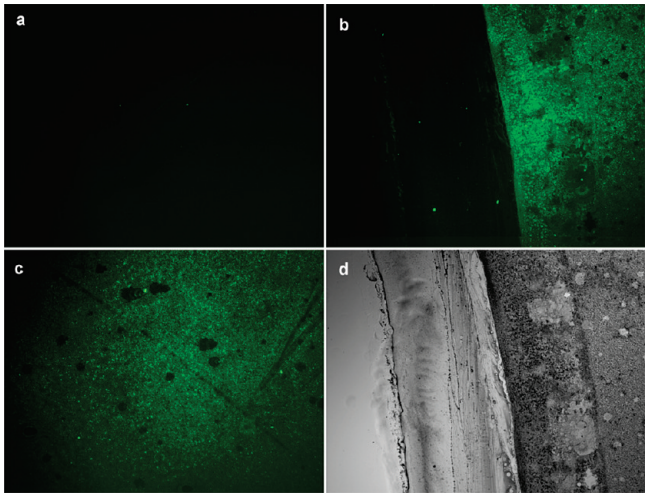

FIGURE 3. Fluorescence images of (a) a bare ITO electrode, (b) the boundary of the PPPA film, (c) a bulk PPPA film and the bright-field image of (d) the boundary of the PPPA film.

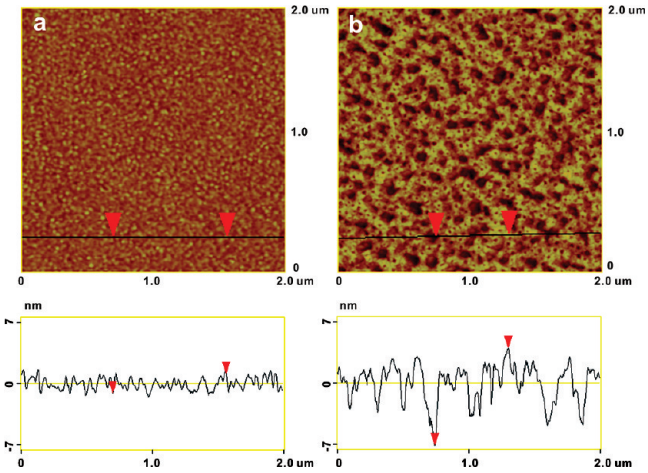

FIGURE 4. AFM images (2 × 2 μm) and section analysis of (a) a control gold surface and (b) the PPPA film. The PPPA film was prepared by CV scans for one cycle in the potential range of −0.3 to +0.75 V vs SCE.

plane and out-of-plane deformation vibrations. The distinct peak at 1728 cm^{-1} resulted from C═O vibration adsorption, verifying the existence of −COOH groups in the PPA monomer. After electropolymerization, the FTIR spectra of the PPPA film did not show much difference except that the peaks in the range of 1500−700 cm^{-1} were not so well-defined in comparison to those of the PPA monomer, mainly because of interactions or steric effects between compact pyrrole rings. However, the characteristic peak of −COOH at 1728 cm^{-1} was not weakened like other peaks. This demonstrates that the −COOH groups were not involved in the electropolymerization process and still available for postmodification.

In our work, the morphology of the PPPA film was observed using SEM and AFM. The SEM image (Figure S4 in the Supporting Information) displayed the cauliflower-like shape of the PPPA film, while AFM images exhibited its finer surface structure, as illustrated in Figure 4. The clean gold surface showed well-aligned gold atom clusters clearly, and its surface roughness was less than 2.2 nm. In contrast, the PPPA film showed a porous structure with an aperture size of 0.2−0.5 μm, and the surface roughness increased to 11.1 nm. Correspondingly, the contact angle also changed from 72.2° for the bare gold surface to 27.0° for the PPPA-coated surface, indicative of the high hydrophilicity of the PPPA film.

3.2. Possible Applications of the PPPA Film in Sensors. The PPPA film, as a functional material, shows some unique properties for chemical and biological sensor applications. For example, the nanoporous structure and hydrophilic behavior imply its function as permeable and permselective membranes; the abundant −COOH functional groups located in the polymer backbone make it an ideal matrix for biomolecule immobilization; the nature of the PPPA film as a fluorescent polyanionic material qualifies its use in optical sensors. Detailed discussions on the three points are presented in the following subsections individually.

3.2.1. Permeable and Permselective Membranes. The most common role of the polymer film in sensors is to act as a variable resistance to the passage of permeating species, with the property characterized by permeability and permselectivity. Permeability is a measure of the rate at which a given species permeates a polymeric barrier, while permselectivity is a measure of the rates of two or more species relative to one another (1). Various techniques have evolved for measuring these two parameters. In our study, the permeability and permselectivity of the PPPA film was investigated by RDE voltammetry using $Fe(CN)_6^{3-}/Fe(CN)_6^{4-}$ as probes (24−27). As documented by Gough and Leypoldt (28) (see the Supporting Information for a further explanation), the steady-state limiting current of $Fe(CN)_6^{3-}$ and $Fe(CN)_6^{4-}$ ions on a PPPA-coated electrode can be expressed as

$$\frac{1}{i_{\mathrm{lim}}} = \frac{1}{0.62nFAD_{\mathrm{s}}^{2/3}C\nu^{-1/6}\omega^{1/2}} + \frac{\delta}{nFAKCD_{\mathrm{m}}} \qquad (1)$$

where i_{lim} is the steady-state limiting current, A is the electrode area, D_{s} is the diffusion coefficient for the substrate in solution, $C°$ is the concentration in the bulk of the solution, ν is the kinematics viscosity of the solution, D_{m} is the diffusion coefficient of the substrate in the polymer, K is the equilibrium partition coefficient, ω is the rotation rate of RDE, and δ is the thickness of the polymer film. From eq 1, it is obvious that a plot of $1/i_{\mathrm{lim}}$ versus $1/\omega^{1/2}$ (Koutecky−Levich plot) should be a straight line with a positive intercept $\delta/(nFAD_{\mathrm{m}}KC°)$, whose value relies on the permeability constant of the polymer film ($P_{\mathrm{m}} = D_{\mathrm{m}}K$). Figure 5 gives the RDE voltammograms obtained at bare and PPPA-coated gold electrodes in a 5 mmol/L $Fe(CN)_6^{3-}/Fe(CN)_6^{4-}$ solution. As expected, the experimental data of a PPPA-coated electrode ($1/i_{\mathrm{lim}} \sim 1/\omega^{1/2}$) showed a linear relationship with the same slope as that for the bare electrode. The permeability constants of $Fe(CN)_6^{4-}$ and $Fe(CN)_6^{3-}$ were calculated from the intercept as 1.03×10^{-7} and 1.41×10^{-7} cm^2/s, respectively. Table 2 lists the permeability values of some inorganic and polymer films claimed in the literature using

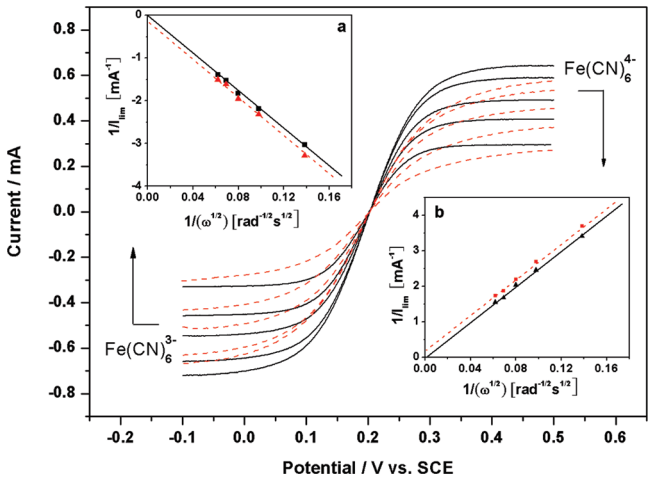

FIGURE 5. RDE voltammograms of a PPPA-coated gold electrode (d = 5 mm) in a PBS solution (pH = 7.4) containing 5 mM $Fe(CN)_6^{3-}$/$Fe(CN)_6^{4-}$. The rotating speeds are 500, 1000, 1500, 2000, and 2500 rpm/min, respectively. Scan rate: 0.2 mV/s. Solid line: bare gold electrode. Dashed line: PPPA-coated gold electrode. (Inset a) Reciprocal of the steady-state limiting anodic current versus the reciprocal of the square root of the rotation rate (Koutecky−Levich plot) at a bare gold electrode (solid line) and a PPPA-coated electrode (dashed line). (Inset b) Koutecky−Levich plot of the cathodic current at a bare gold electrode (solid line) and a PPPA-coated electrode (dashed line). Thickness of the film: 24 nm.

Table 2. Permeability Values of Some Inorganic and Organic Films

materials	permeating species	permeability constant/ $cm^2\ s^{-1}$	ref
poly(triaminophenanthroline iron)	$Fe(CN)_6^{4-}$/0.9 nm	2.6×10^{-9}	28
mesoporous silica film	$Ru(bpy)_3^{2+}$/1.1 nm	2.0×10^{-8}	29
poly(vinyl diquat)	$Ru(bpy)_3^{2+}$/1.1 nm	1.3×10^{-9}	30
poly(trivinylbipyridinylruthenium)	ferrocene/1.0 nm	1.2×10^{-8}	31
poly(cobalt porphyrin)	ferrocene/1.0 nm	8.2×10^{-8}	32
poly(*o*-aminophenol)	$Fe(CN)_6^{4-}$/0.9 nm	3.9×10^{-9}	33
polypyrrole	$Fe(CN)_6^{3-}$/0.9 nm	1.3×10^{-9}	34

permeating species with sizes similar to that of $Fe(CN)_6^{3-}$/$Fe(CN)_6^{4-}$. It can be found that the permeability of the PPPA film is 1 order or even 2 orders higher than those reported for other films, resulting from the high hydrophilicity and rich nanopores formed in the PPPA film. Note that the permeability of the PPPA film can be adjusted by controlling its porosity during the fabrication process; for instance, the nanopores obtained from the galvanostatic method were always larger than those from CV. Besides, the difference of the permeability constant between $Fe(CN)_6^{4-}$ and $Fe(CN)_6^{3-}$ implies the permselectivity of the PPPA film to the two ions. This can be ascribed to the electrostatic repulsion between the PPPA film (negative charge) and $Fe(CN)_6^{4-}$/$Fe(CN)_6^{3-}$, which imposes a stronger repulsive force to $Fe(CN)_6^{4-}$ than $Fe(CN)_6^{3-}$. On the contrary, the permeation of cations can be accelerated by the electrostatic affinity (data not shown here). As a consequence, the PPPA film may exhibit a strong selectivity to cations over anions. In addition to electrostatic interactions, the presence of −COOH groups also allows postmodification to introduce ionophores so that the permselectivity of the PPPA film could be further enhanced. These features provide the possible utilization of the PPPA film as an ion-separation membrane in an ion-selective electrode/sensor to improve their selectivity to a certain ion type or as a diffusion membrane in amperometric electrochemical sensors (35, 36).

3.2.2. Matrix for Biomolecule Immobilization.

The search for suitable methods to immobilize probe biomolecules like proteins, DNAs, and cells is a key subject in biosensor construction (37−40). In spite of much effort in this field, stable and reproducible immobilization of biomolecules with complete retention of their recognition properties still remains a crucial problem for the commercialization of biosensors. One promising solution is to use biocompatible polymers as a matrix for biomolecule immobilization. Several physical and chemical techniques have been developed to immobilize biomolecules onto a polymer surface, i.e., physical adsorption onto a polymer surface (41), covalent binding between biomolecules and polymers (42), entrapment of a biomolecule into a "cage" or polymer gel (43), and so on. For covalent binding, carboxyl-functionalized polymers like PPPA are especially favorable because of their capability forming an amide bond with amino groups in peptides and proteins. Moreover, electropolymerization of the PPPA film enables addressable deposition of the polymer film and, therefore, provides precise control of biomolecule immobilization on surfaces with high spatial resolution. In our study, anti-mouse IgG (protein) was employed to investigate the possibility of the PPPA film as a polymer matrix for biomolecule immobilization. The results were characterized using AFM because of its ability to maintain the bioactivity of biomolecules during the measurement. Figure 6a shows the AFM images of the PPPA film after anti-mouse IgG immobilization. Compared with the bare PPPA film (Figure 4b), the morphology of the protein-modified PPPA film changed dramatically. The porous structure vanished, and the surface was packed with a number of small particles, which could be assigned to anti-mouse IgG. The abundant amount of immobilized anti-mouse IgG implies the high quantity and good accessibility of specific recognition sites on the treated PPPA film surface. Normally, the covalent binding method often suffers from the low bioactivity of attached probe biomolecules, leading to poor interaction between the probe and analyte and thus a decrease in the sensing performance (44). Here the bioactivity of immobilized anti-mouse IgG was detected by mouse IgG via antibody/antigen interactions. As can be seen from Figure 6b, particles with bigger size appeared after incubation with mouse IgG and the surface roughness increased from 8 to 15 nm accordingly. The average particle size in Figure 6b was measured as ~14 nm, in accordance with the size of mouse IgG. The large magnitude and round shape of mouse IgG reveals that the incubated mouse IgG preserves its nature quite well and thus proves the high bioactivity of the immobilized antibody, anti-mouse IgG. It should be mentioned that biomolecules can also be entrapped in the PPPA film during the electrogeneration process and their bioactivity is retained to a large extent (data not shown here). The amount of specific recognition sites on the PPPA film is adjustable by codeposition of other conducting polymers

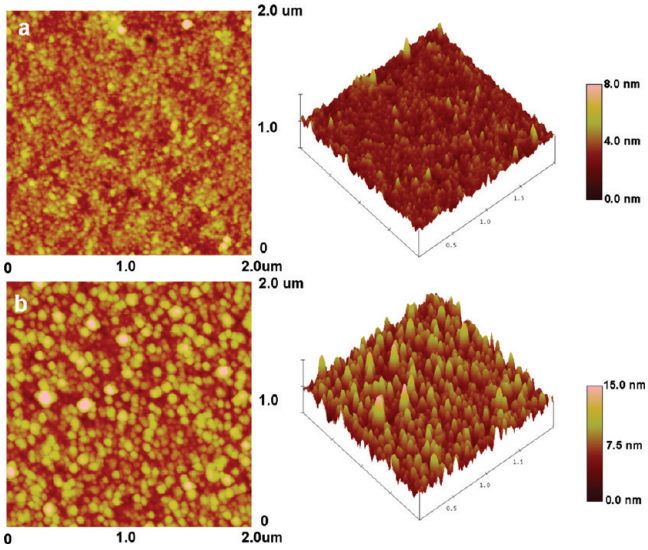

FIGURE 6. AFM images of the PPPA film surface (2 × 2μm) after immobilization of anti-mouse IgG (a) and subsequent incubation of mouse IgG (b). The whole procedure was described as below: 150 μL each of ~2 mmol/L EDC and ~5 mmol/L NHS was added after PPA electropolymerization and reacted for 1 h at room temperature. After washing three times with PBS, 1 μg/mL of an anti-mouse IgG solution was added and incubated for 2 h. Then the surface was washed again to remove unreacted anti-mouse IgG. Part a was captured at this stage. In order to occupy the residual specific recognition sites and reduce the nonspecific adsorption, a bovine serum albumin blocking treatment was performed and followed by rinsing with PBS. Thereafter, 1 μg/mL of mouse IgG was added and incubated for 2 h. Part b was captured after washing with PBS.

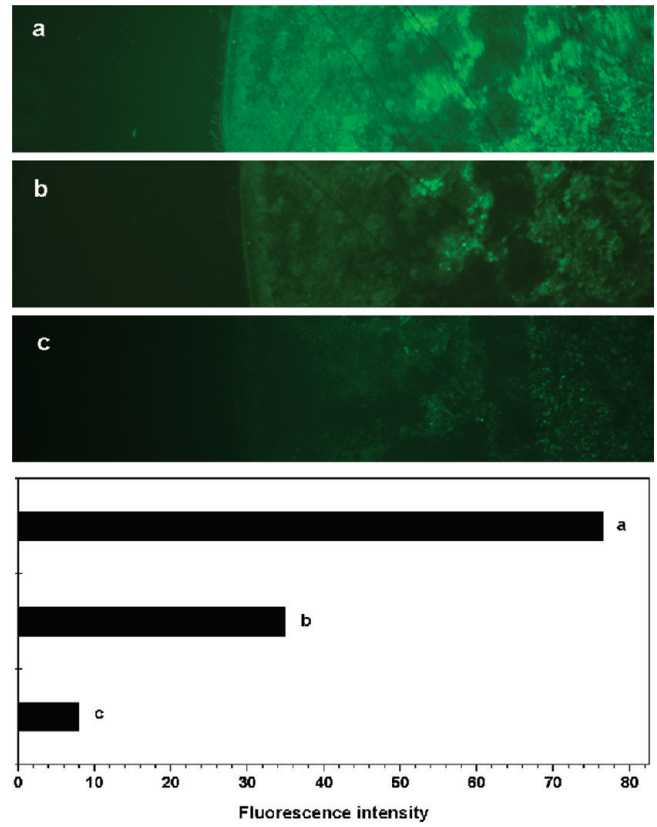

FIGURE 7. Comparison of the fluorescence intensities of the PPPA film before and after the addition of MV^{2+}: (a) PPPA film in an aqueous solution (pH = 6.8) without MV^{2+}; (b) PPPA film in an aqueous solution (pH = 6.8) containing 1 mmol/L MV^{2+}; (c) PPPA film in an alkaline solution (pH = 10) containing 1 mmol/L MV^{2+}. The high fluorescence background was caused by the light scattering of the glass container and the aqueous medium.

without functionalized groups in a certain ratio (45). This experiment shows vividly that the PPPA film can be used in biosensors as an ideal matrix for biomolecule immobilization.

3.2.3. Fluorescent Conjugated Polymer. The use of fluorescent conjugated polymers in chemical and biological sensors was first discovered by Zhou and Swager (46), who found that the transfer of excitation energy along the backbone of conjugated polymers to the chromophore reporter would result in amplification of the fluorescence signals. A number of water-soluble polymers such as poly(*p*-phenylenevinylene)s, poly(thiophene)s, poly(phenyleneethynylene)s, polyfluorenes, etc., have been widely explored, and many kinds of chemical sensors (e.g., TNT sensor, H_2O_2 sensor, etc.) and biosensors (e.g., protein sensor, DNA sensor) have been developed so far (47−50). Here we report that the PPPA film, as a water-insoluble fluorescent conjugated polymer, also displays amplification of fluorescence quenching during interaction with an electron-deficient compound: methyl viologen (MV^{2+}). Figure 7 compares the fluorescence images of the PPPA film with and without the presence of MV^{2+}. Because of the light scattering of the glass container and aqueous medium, the fluorescence image of the PPPA film captured in a MV^{2+} solution (Figure 7a) showed a higher background relative to that of the dry PPPA film in Figure 3b. However, it was still observable that the fluorescence intensity decreased with the presence of MV^{2+} (Figure 7b). According to the literature (51, 52), three reasons may interpret this phenomenon:

Scheme 1. Chemical Synthesis Route of PPPA Monomer and Polymer

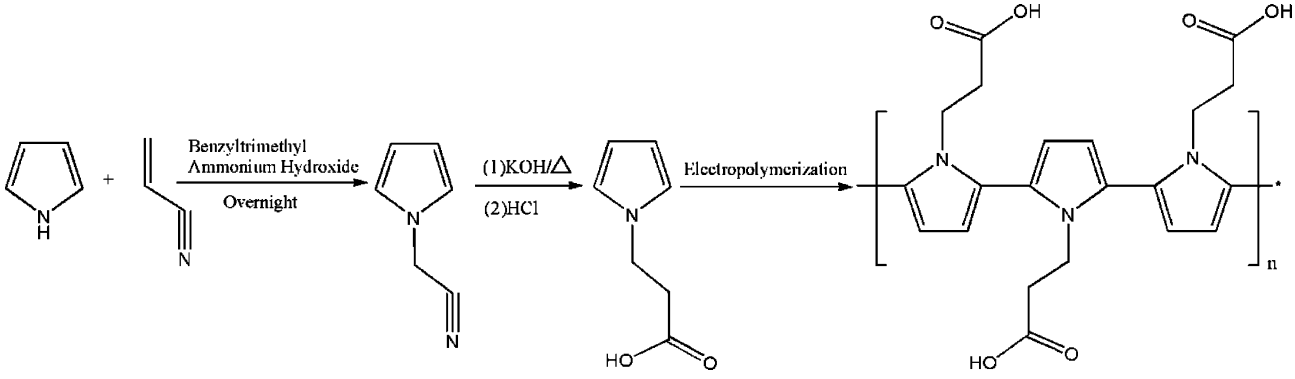

photoinduced electron transfer, analyte-induced aggregation of the conjugated polymer, and analyte-induced conformational changes. Obviously, analyte-induced aggregation and conformational changes do not come into existence because of the solid state of the PPPA film and thus cannot account for our experiment results. Therefore, fluorescence quenching of the PPPA film can only be explained as photoinduced electron transfer. Because PPPA is a polyanionic polymer, the addition of MV^{2+} can cause the formation of a PPPA/MV^{2+} complex via electrostatic interaction and thus produce the trapping sites for the excitation. The conjugated PPPA polymer backbone allows efficient delocalization of the electronic excited state (exciton) and ultrafast exciton mobility along the conjugated polymer chain. When excited, almost all of the exciton energy can be trapped by the bound quencher MV^{2+}. Here the binding degree of PPPA and MV^{2+} plays a significant role in the quenching efficiency (53). In a neutral medium, the electrostatic interaction between PPPA and MV^{2+} was not very strong because of the low ionization of −COOH groups in the PPPA film, leading to the relatively low quenching efficiency (46%; Figure 7b). However, with growth of the pH value, the ionization of −COOH groups became higher so as to enhance the electrostatic interaction with MV^{2+}, by which an efficient exciton migration channel to the quencher was established (Figure 7c). As a result, the fluorescence intensity in the alkaline medium fell to ca. 10% of the original value. A lower concentration of MV^{2+} such as 0.1 mM was also tested, and the results were quite similar to what we reported here, implying high quenching sensitivity. It is worth noting that the nanoporous structure of the PPPA film also favors permeation of MV^{2+} into the bulk of the polymer film, and thus the PPPA/MV^{2+} complex can be formed in the whole film and is not just limited to the outermost surface. On the basis of the fluorescence superquenching properties of the PPPA film, a lot of chemical and biological sensors can be constructed to detect different analytes.

4. CONCLUSIONS

Briefly, we synthesized the PPPA film via an electrochemical method and characterized it using confocal-Raman/fluorescence microscopy, AFM, SEM, FTIR, and contact-angle measurements. Confocal-Raman microscopy proves that the chain length of the PPPA polymer varies with progress of the electropolymerization process; i.e., the highest chain length appears at the electrode/polymer interface and gradually decreases with growth of the PPPA film. Fluorescence microscopy demonstrates its strong fluorescence emission. AFM and SEM images identify the unique nanoporous structure of the PPPA film. FTIR data confirm the presence of abundant −COOH functional groups in the polymer backbone, and contact-angle tests show the high hydrophilicity of the polymer film. On the basis of these unique properties, three potential applications of the PPPA film in chemical and biological sensors are proposed and investigated: (1) permeable and permselective membranes (the RDE measurement shows that the permeability of the PPPA film is about 1 order or even 2 orders higher than that of the other polymers, and good permselectivity can be realized for the ions with different charges); (2) matrix for biomolecule immobilization (AFM characterization of protein immobilization on the PPPA film via covalent binding mode demonstrates that high magnitude of biomolecules can be attached to the polymer surface and their bioactivity is maintained quite well); (3) fluorescent conjugated polymer (the amplification of fluorescence quenching is achieved by the addition of an electron-deficient compound: MV^{2+}). The high quenching efficiency in the alkaline medium results from strong electrostatic interactions between PPPA polymer and MV^{2+}.

Acknowledgment. Part of this work was financially supported by the Center for Advanced Bionanosystems, Nanyang Technological University, Singapore.

Supporting Information Available: The experimental data for UV−vis, FTIR, SEM, and contact-angle measurement, 3D figure of fluorescence emission in the PPPA film, detailed setting of RDE and confocal Raman microscopy, theory for the use of RDE technology to study the permeability and permselectivity of the PPPA film. This material is available free of charge via the Internet at http://pubs.acs.org.

REFERENCES AND NOTES

(1) Harsányi, G. *Polymer films in sensor applications*; CRC Press: Boca Raton, FL, 1995.
(2) Harsányi, G. *Sensor Rev.* **2000**, *20*, 98.
(3) Li, C. M.; Dong, H.; Cao, X. D.; Luong, J. H. T.; Zhang, X. J. *Curr. Med. Chem.* **2007**, *14*, 937.
(4) Ramanavičius, A.; Ramanavičiene, A.; Malinauskas, A. *Electrochim. Acta* **2006**, *51*, 6025.
(5) Zotti, G.; Zecchin, S.; Schiavon, G.; Vercelli, B.; Berlin, A.; Grimoldi, S. *Macromol. Chem. Phys.* **2004**, *205*, 2026.
(6) Wang, W. Q.; Yu, D. M.; Tian, F. *Synth. Met.* **2008**, *158*, 717.
(7) Mao, C.; Zhu, A. P.; Wu, Q.; Chen, X. B.; Kim, J. H.; Shen, J. *Colloids Surf. B* **2008**, *67*, 41.
(8) Roux, S.; Duwez, A. S.; Demoustier-Champagne, S. *Langmuir* **2003**, *19*, 306.
(9) Hiller, M.; Kranz, C.; Huber, J.; Bäuerle, P.; Schuhmann, W. *Adv. Mater.* **1996**, *8*, 219.
(10) Lee, J. W.; Serna, F.; Nickels, J.; Schmidt, C. E. *Biomacromolecules* **2006**, *7*, 1692.
(11) Dong, H.; Li, C. M.; Chen, W.; Zhou, Q.; Zeng, X. Z.; Luong, J. H. T. *Anal. Chem.* **2006**, *78*, 7424.
(12) Blume, R. C.; Lindwall, H. G. *Org. Chem.* **1945**, *10*, 255.
(13) Wolowacz, S. E.; Yon Hin, B. F. Y.; Lowe, C. R. *Anal. Chem.* **1992**, *64*, 1541.
(14) Scherf, U.; List, E. J. W. *Adv. Mater.* **2002**, *14*, 477.
(15) Bliznyuk, V. N.; Carter, S. A.; Scott, J. C.; Klärner, G.; Miller, R. D.; Miller, D. C. *Macromolecules* **1999**, *32*, 361.
(16) Lammi, R. K.; Barbara, P. F. *Photochem. Photobiol. Sci.* **2005**, *4*, 95.
(17) Jennings, P.; Jones, A. C.; Mount, A. R. *J. Chem. Soc., Faraday Trans.* **1998**, *94*, 3619.
(18) Argyrakis, P.; Kobryanskii, M. V.; Sluch, M. I.; Vitukhnovsky, A. G. *Synth. Met.* **1997**, *91*, 159.
(19) Sacristan, J.; Mijangos, C.; Reinecke, H.; Spells, S.; Yarwood, J. *Macromol. Rapid Commun.* **2000**, *21*, 894.
(20) Michielsen, S. *J. Appl. Polym. Sci.* **2001**, *81*, 1662.
(21) Li, N. J.; Lu, J. M.; Yao, S. C.; Xia, X. W.; Zhu, X. L. *Mater. Lett.* **2004**, *58*, 3115.
(22) Vanden Bout, D. A.; Yip, W. T.; Hu, D.; Fu, D. K.; Swager, T. M.; Barbara, P. F. *Science* **1997**, *277*, 1074.
(23) Hu, D.; Yu, J.; Wong, K.; Bagchi, B.; Rossky, P. J.; Barbara, P. F. *Nature* **2000**, *405*, 1030.
(24) Leddy, J.; Bard, A. *J. Electroanal. Chem.* **1983**, *153*, 223.
(25) Savéant, J. M. *J. Electroanal. Chem.* **1991**, *302*, 91.

(26) Hofér, E.; Steckhan, E.; Ramos, B.; Heineman, W. R. *J. Electroanal. Chem.* **1996**, *402*, 115.
(27) Ionescu, R. E.; Gondran, C.; Gheber, L. A.; Cosnier, S.; Marks, R. S. *Anal. Chem.* **2004**, *76*, 6808.
(28) Gough, D. A.; Leypoldt, J. K. *Anal. Chem.* **1979**, *51*, 439.
(29) Massari, A. M.; Gurney, R. W.; Schwartz, C. P.; Nguyen, S. T.; Hupp, J. T. *Langmuir* **2004**, *20*, 4422.
(30) Etienne, M.; Quach, A.; Grosso, D.; Nicole, L.; Sanchez, C.; Walcarius, A. *Chem. Mater.* **2007**, *19*, 844.
(31) Ikeda, T.; Schmehl, P.; Denisevich, P.; Willman, K.; Murry, R. W. *J. Am. Chem. Soc.* **1982**, *104*, 2683.
(32) Pressprich, K. A.; Maybury, S. G.; Thomas, R. E.; Linton, R. W.; Irene, E. A.; Murray, R. W. *J. Phys. Chem.* **1989**, *93*, 5568.
(33) Bonfranceschi, A.; Pérez Córdoba, A.; Keunchkarian, K.; Zzapata, S.; Tucceri, R. *J. Electroanal. Chem.* **1999**, *477*, 1.
(34) Gros, P.; Gibson, T.; Bergel, A.; Comtat, M. *J. Electroanal. Chem.* **1997**, *437*, 125.
(35) Dong, H.; Cao, X. D.; Li, C. M. *Biosens. Bioelectron.* **2008**, *23*, 1055.
(36) Dong, H.; Li, C. M.; Zhang, Y. F.; Cao, X. D.; Gan, Y. *Lab Chip* **2007**, *7*, 1752.
(37) Ahuja, T.; Mir, I. A.; Kumar, D.; Rajesh. *Biomaterials* **2007**, *28*, 791.
(38) Ding, L.; Du, D.; Zhang, X. J.; Ju, H. X. *Curr. Med. Chem.* **2008**, *15*, 3160.
(39) Arya, S. K.; Datta, M.; Malhotra, B. D. *Biosens. Bioelectron.* **2008**, *23*, 1083.
(40) MacBeath, G.; Schreiber, S. L. *Science* **2000**, *289*, 1760.
(41) Zhou, D. J.; Wang, X.; Birch, L.; Rayment, T.; Abell, C. *Langmuir* **2003**, *19*, 10557.
(42) Yang, T.; Jung, S. Y.; Mao, H.; Cremer, P. S. *Anal. Chem.* **2001**, *73*, 165.
(43) Liang, R. P.; Jiang, J. L.; Qiu, J. D. *Electroanalysis* **2008**, *20*, 2642.
(44) Cosnier, S. *Appl. Biochem. Biotechnol.* **2000**, *89*, 127.
(45) Hu, W. H.; Li, C. M.; Cui, X. Q.; Dong, H.; Zhou, Q. *Langmuir* **2007**, *23*, 2761.
(46) Zhou, Q.; Swager, T. M. *J. Am. Chem. Soc.* **1995**, *117*, 12593.
(47) McQuade, D. T.; Pullen, A. E.; Swager, T. M. *Chem. Rev.* **2000**, *100*, 2537.
(48) Thomas, S. W., III; Joly, G. D.; Swager, T. M. *Chem. Rev.* **2007**, *107*, 1339.
(49) Liu, B.; Bazan, G. C. *Chem. Mater.* **2004**, *16*, 4467.
(50) Chen, L. H.; McBranch, D. W.; Wang, H. L.; Helgeson, R.; Wudl, F.; Whitten, D. G. *Proc. Natl. Acad. Sci. U.S.A.* **1999**, *96*, 12287.
(51) Feng, F. D.; He, F.; An, L. L.; Wang, S.; Li, Y. L.; Zhu, D. B. *Adv. Mater.* **2008**, *20*, 2959.
(52) Wang, J.; Wang, D. L.; Miller, E. K.; Moses, D.; Bazan, G. C.; Heeger, A. J. *Macromolecules* **2000**, *33*, 5153.
(53) He, F.; Tang, Y. L.; Yu, M. H.; Wang, S.; Li, Y. L.; Zhu, D. B. *Adv. Funct. Mater.* **2006**, *16*, 91.

AM900267E